# Non-Markovian Modeling of Nonequilibrium Fluctuations and Dissipation in Active Viscoelastic Biomatter

Amir Abbasi,[1] Roland R. Netz,[1] and Ali Naji[2,3,*]
[1]Fachbereich Physik, Freie Universität Berlin, Arnimallee 14, 14195 Berlin, Germany
[2]School of Nano Science, Institute for Research in Fundamental Sciences (IPM), Tehran 19538-33511, Iran
[3]Department of Physics, College of Science, Sultan Qaboos University, Muscat 123, Oman

(Received 22 July 2022; accepted 19 October 2023; published 30 November 2023)

Based on a Hamiltonian that incorporates the elastic coupling between a tracer particle and the embedding active viscoelastic biomatter, we derive a generalized non-Markovian Langevin model for the nonequilibrium mechanical tracer response. Our analytical expressions for the frequency-dependent tracer response function and the tracer positional autocorrelation function agree quantitatively with experimental data for red blood cells and actomyosin networks with and without adenosine triphosphate over the entire frequency range and in particular reproduce the low-frequency violation of the fluctuation-dissipation theorem. The viscoelastic power laws, the elastic constants and effective friction coefficients extracted from the experimental data allow straightforward physical interpretation.

DOI: 10.1103/PhysRevLett.131.228202

Viscoelastic gels such as permanently or transiently cross-linked networks of semiflexible polymers constitute important soft biological materials [1–3]. The polymeric nature of such gels is responsible for their salient rheological properties. The cell cytoskeleton is a prime example of a viscoelastic gel [4,5] and determines cell shape, motility, and division [6,7]. Even though the cytoskeleton has a complex structure, its mechanical properties at small deformations are determined mainly by the underlying F-actin network [8,9]. Even in equilibrium (EQ), the dynamic properties of F-actin are complex [10]. *In vivo*, constant F-actin (de)polymerization and interactions with myosin motors consume adenosine triphosphate (ATP) and drive the viscoelastic network into a nonequilibrium (NEQ) state [11–13], where the motors act as active cross-links and produce local tension [2].

Another illustrious example of active viscoelastic biomatter are red blood cells (RBCs), whose structural components include a filamentous protein (spectrin) scaffold underneath the enclosing cell membrane [14–18]. The mechanical response and spectra of membrane fluctuations (RBC flickering) display NEQ signatures due to the membrane ion-pump activity and the ATP-induced spectrin network reorganization [19–21].

Supported by high-resolution experimental data [13,18,20,22–26], a key line of inquiry has been to examine violations of the fluctuation-dissipation theorem (FDT) in these NEQ systems. The FDT holds for near-EQ dynamical processes but not in NEQ, as indeed corroborated by microrheology experiments [13,20]. Typical experiments involve a micron-sized tracer bead immersed in the active medium whose motion is tracked and which is either allowed to move spontaneously or is driven by a laser beam (passive versus active microrheology). Active microrheology allows us to simultaneously measure the mechanical response and the positional autocorrelation function and thereby to check the validity of the FDT.

Theoretical studies of FDT violation focused on externally forced systems [27–29], glasses [30], and active systems [13,20,31]. NEQ fluctuations have been modeled by an additive athermal noise acting on particles in a viscous fluid [21,32]. A similar strategy has been used to model active dynamical undulations of elastic biological membranes [21,33–35] and several computational models have explicitly incorporated active pumps [20,36]. A NEQ elastic model for the interaction of motors and a tracer particle was recently shown to describe the frequency dependence of the experimentally observed FDT violation [13] rather well [37].

In this Letter, we model the NEQ mechanical response of a tracer particle that is embedded in an active biogel by taking into account the gel viscoelasticity and the elastic coupling between the tracer and the gel. We derive analytical spectral expressions for the tracer response to an external applied force and the tracer position correlation functions. By simultaneously fitting both functions to experimental microrheological data for RBCs [20] and reconstituted actomyosin networks [13], we extract all parameters describing the active viscoelastic gel and the

elastic coupling between tracer and gel. We find that power-law viscoelasticity describes the experimental data better than the standard Maxwell and Kelvin-Voigt viscoelastic models. The extracted viscoelastic exponent is close to $\kappa = 3/4$ for actomyosin networks and close to unity for RBC, in agreement with previous studies. Interestingly, ATP increases the effective temperature ratio between the active gel and the tracer to above 20 for both systems, demonstrating that ATP drives these systems very far from EQ. The quantitative agreement established with experiments demonstrates the generic capability of our multicomponent model that combines elastic interactions and active viscoelasticity into a single framework and enables closed-form predictions of tracer-response and correlation spectra.

Inspired by typical microrheology experiments [13,20,24], we assume a single tracer bead of mass $M$ that is coupled elastically via harmonic springs of strength $k$ to $n$ coordinates in the gel characterized by mass $m$. The tracer is trapped in a harmonic potential of elastic constant $K$. The Hamiltonian reads

$$H = \frac{K}{2}X^2 + \frac{M}{2}\dot{X}^2 + \sum_{i=1}^{n}\frac{k}{2}(X - x_i)^2 + \sum_{i=1}^{n}\frac{m}{2}\dot{x}_i^2, \quad (1)$$

where $X$ is the position of the tracer and $x_i$ are the gel coordinates ($i = 1, \ldots, n$), $\dot{X}$ and $\dot{x}_i$ are the tracer and gel velocities. We assume that the system is isotropic and therefore use one-dimensional displacement variables, the extension to multidimensional variables is straightforward [37,38]. The system dynamics is assumed to follow generalized Langevin equations (GLE), which, in addition to the deterministic forces from the Hamiltonian, contain thermal and active random forces as well as time-dependent friction forces due to the viscoelasticity of the gel. The latter is modeled using a general friction kernel $\mathcal{K}_+(t)$ [39,40], yielding the GLEs

$$M\ddot{X}(t) = -\gamma\int_{-\infty}^{t} dt'\,\mathcal{K}_+(t-t')\dot{X}(t') - (nk+K)X(t) + k\sum_i x_i(t) + F(t), \quad (2a)$$

$$m\ddot{x}_i(t) = -\gamma_a\int_{-\infty}^{t} dt'\,\mathcal{K}_+(t-t')\dot{x}_i(t') - k[x_i(t) - X(t)] + f_i(t). \quad (2b)$$

Here, $\gamma$ and $\gamma_a$ are drag coefficients and $F(t)$ and $f_i(t)$ are random forces acting on the tracer and the active gel coordinates, respectively, with zero mean and second moments given by $\langle F(t)F(t')\rangle = k_B T\gamma\mathcal{K}_+(|t-t'|)$ and $\langle f_i(t)f_j(t')\rangle = k_B T_a\gamma_a\delta_{ij}\mathcal{K}_+(|t-t'|)$. Note that the friction kernels of the tracer and the gel coordinates are approximated to be identical and given by $\mathcal{K}_+(t)$, which reflects that the gel viscoelasticity dominates the friction of both components. Based on previous results for biological membranes and gels [13,41–45], we use a normalized power-law memory kernel, $\mathcal{K}_+(t) = t^{-\kappa}/\Gamma(1-\kappa)$, where $\Gamma(x)$ is the Gamma function. In Supplemental Material, Sec. I [46], we demonstrate that the power-law viscoelastic model describes experimental data better than other viscoelastic models. In Supplemental Material, Sec. II [46], we extract the memory function directly from the experimental response function and obtain good agreement with our power-law ansatz. In EQ, the temperatures characterizing the random forces $T_a$ and $T$, are equal. In our model NEQ is induced by choosing $T_a \neq T$, the single parameter $\alpha = T_a/T - 1$ thus quantifies the deviation from EQ [37]. In Supplemental Material, Sec. III [46], we test a more elaborate model with an additional exponentially decaying component in the correlation of the active noise acting on the gel [21]. There, we show that the description of the experimental data is not significantly improved and that the product of the exponential decay time of the active noise correlation and the squared noise strength plays a similar role as $\alpha$ [46].

By summing over the gel coordinates and introducing collective variables $x(t) = \sum_i x_i(t)/n$ and $f(t) = \sum_i f_i(t)/n$, we obtain two coupled GLEs

$$M\ddot{X}(t) = -\gamma\int_{-\infty}^{t} dt'\,\mathcal{K}_+(t-t')\dot{X}(t') - (nk+K)X(t) + nkx(t) + F(t), \quad (3a)$$

$$m\ddot{x}(t) = -\gamma_a\int_{-\infty}^{t} dt'\,\mathcal{K}_+(t-t')\dot{x}(t') - k[x(t) - X(t)] + f(t), \quad (3b)$$

for the tracer and the collective gel coordinate. The gel random noise has zero mean and strength $\langle f(t)f(t')\rangle = k_B T_a\gamma_a\mathcal{K}_+(|t-t'|)/n$. Equation (3) can be solved in terms of the Fourier-transformed tracer position $\tilde{X}(\omega) = \int dt\, X(t)e^{i\omega t}$ to yield

$$\tilde{X}(\omega) = \frac{\tilde{F}_R(\omega)}{-M\omega^2 - i\omega\tilde{\mathcal{K}}_{tot}(\omega) + K}, \quad (4)$$

with the effective friction kernel and the effective noise given by

$$\tilde{\mathcal{K}}_{tot}(\omega) = \left[\gamma\tilde{\mathcal{K}}_+(\omega) + \frac{nk\gamma_a\tilde{\mathcal{K}}_+(\omega)}{-i\omega\gamma_a\tilde{\mathcal{K}}_+(\omega) + k}\right], \quad (5)$$

$$\tilde{F}_R(\omega) = \frac{nk\tilde{f}(\omega)}{-i\omega\gamma_a\tilde{\mathcal{K}}_+(\omega) + k} + \tilde{F}(\omega). \quad (6)$$

From Eq. (4) we can directly calculate the tracer positional autocorrelation function, $\tilde{C}(\omega) = \int dt\langle X(0)X(t)\rangle e^{i\omega t}$, and

the imaginary part of the response function $\tilde{\chi}''(\omega)$, defined by the linear-response relation $X(t) = \int_0^\infty dt' \chi(t-t') F_R(t')$ (see derivation in Supplemental Material, Sec. IV, and resulting expressions for different viscoelastic memory kernels in Sec. V of [46]). The FDT violation can be quantified by the spectral function [37]

$$\Xi(\omega) = \frac{\omega \tilde{C}(\omega)/(2k_B T)}{\tilde{\chi}''(\omega)} - 1 = \frac{\tilde{C}_F(\omega)/(2k_B T)}{\tilde{\mathcal{K}}'_{\rm tot}(\omega)} - 1, \quad (7)$$

where $\tilde{C}_F(\omega) = \int dt \langle F_R(0) F_R(t) \rangle e^{i\omega t}$ is the spectral noise autocorrelation and $\tilde{\mathcal{K}}'_{\rm tot}(\omega)$ the real part of the Fourier-transformed memory kernel. For an equilibrium system characterized by $\alpha = 0$, i.e., when the tracer and the gel have the same temperature, the FDT is recovered [55] and $\Xi(\omega) = 0$. Assuming overdamped motion with $M \to 0$ and $m \to 0$, we obtain explicitly

$$\tilde{\chi}''(\omega) = \omega^\kappa \sin\left(\frac{\kappa\pi}{2}\right) \left[ (\gamma + \hat{\gamma}_a)\hat{k}^2 + 2\gamma\hat{\gamma}_a \hat{k} \cos\left(\frac{\kappa\pi}{2}\right)\omega^\kappa + \gamma\hat{\gamma}_a^2 \omega^{2\kappa} \right] \Big\{ \hat{k}^2 K^2 + \gamma^2 \hat{\gamma}_a^2 \omega^{4\kappa} + \left[ 2\gamma\hat{\gamma}_a \hat{k} K \cos(\kappa\pi) + \left(\hat{\gamma}_a(\hat{k}+K) + \gamma\hat{k}\right)^2 \right] \omega^{2\kappa} + 2\cos\left(\frac{\kappa\pi}{2}\right) [\hat{\gamma}_a(\hat{k}+K) + \gamma\hat{k}][\hat{k}K + \gamma\hat{\gamma}_a\omega^{2\kappa}]\omega^\kappa \Big\}^{-1}, \quad (8)$$

$$\tilde{C}(\omega) = 2k_B T \omega^{\kappa-1} \sin\left(\frac{\kappa\pi}{2}\right) \left[ (\gamma + \hat{\gamma}_a(1+\alpha))\hat{k}^2 + 2\gamma\hat{\gamma}_a \hat{k} \cos\left(\frac{\kappa\pi}{2}\right)\omega^\kappa + \gamma\hat{\gamma}_a^2 \omega^{2\kappa} \right] \Big\{ \hat{k}^2 K^2 + \gamma^2 \hat{\gamma}_a^2 \omega^{4\kappa} + \left[ 2\gamma\hat{\gamma}_a \hat{k} K \cos(\kappa\pi) + \left(\hat{\gamma}_a(\hat{k}+K) + \gamma\hat{k}\right)^2 \right] \omega^{2\kappa} + 2\cos\left(\frac{\kappa\pi}{2}\right) [\hat{\gamma}_a(\hat{k}+K) + \gamma\hat{k}][\hat{k}K + \gamma\hat{\gamma}_a\omega^{2\kappa}]\omega^\kappa \Big\}^{-1}, \quad (9)$$

$$\Xi(\omega) = \frac{\hat{\gamma}_a \hat{k}^2 \alpha}{(\gamma + \hat{\gamma}_a)\hat{k}^2 + 2\gamma\hat{\gamma}_a \hat{k} \cos\left(\frac{\kappa\pi}{2}\right)\omega^\kappa + \gamma\hat{\gamma}_a^2 \omega^{2\kappa}}, \quad (10)$$

where the active gel coordinate number $n$ only appears implicitly via $\hat{\gamma}_a = n\gamma_a$ and $\hat{k} = nk$, so we are left with six parameters, the nonequilibrium parameter $\alpha$, the viscoelastic power-law exponent $\kappa$, the tracer and gel drag coefficients $\gamma$ and $\hat{\gamma}_a$, the tracer confinement strength $K$, and the tracer-gel elastic coupling strength $\hat{k}$. We consider two recent microrheology experiments on RBC flickering [20] and cross-linked F-actin networks with myosin II molecular motors [13], both reporting FDT violation by independently measuring $\tilde{\chi}''(\omega)$ and $\tilde{C}(\omega)$. For both experimental systems, it was shown that the FDT remains valid at short times or high frequencies, while strong FDT deviations are observed at long times or low frequencies. We digitize the experimental data for $\tilde{\chi}''(\omega)$ and $\omega\tilde{C}(\omega)/(2k_B T)$ and first fit their high-frequency limits, which from Eqs. (8) and (9) are predicted as $\tilde{\chi}''(\omega) \simeq \sin(\kappa\pi/2)/(\gamma\omega^\kappa)$ and $\omega\tilde{C}(\omega)/(2k_B T) \simeq \sin(\kappa\pi/2)/(\gamma\omega^\kappa)$ and obtain $\kappa$ and $\gamma$ for each dataset. Then, we simultaneous fit Eqs. (8) and (9) in the entire frequency range to find the remaining four parameters, the fitting parameters are shown in Table I, see Supplemental Material, Sec. VI [46], for details on the fitting procedure and the uniqueness of the resulting fit parameters.

We start with the discussion of the RBC data, where flickering dynamics was investigated by tracking the motion of a tracer bead attached to the RBC membrane. In the experiments both the *in vivo* (NEQ) and the ATP-depleted scenarios were considered [20], we denote the latter scenario as EQ although a finite residual ATP concentration is present, as discussed further below. In Figs. 1(a) and 1(b) we find excellent agreement between the experimental data and the fits for $\tilde{\chi}''(\omega)$ and

TABLE I. Model parameters obtained from fits to the experimental data.

| Exp. | $\kappa$ | $\gamma$[pN s$^\kappa$/μm] | $K$[pN/μm] | $\hat{k}$[pN/μm] | $\hat{\gamma}_a$[pN s$^\kappa$/μm] | $\alpha$ |
|---|---|---|---|---|---|---|
| RBC: | | | | | | |
| EQ | $0.926 \pm 0.0655$ | $0.120 \pm 0.00295$ | $5.51 \pm 0.109$ | $1.31 \pm 0.137$ | $0.257 \pm 0.0219$ | $0.985 \pm 0.197$ |
| NEQ | $0.939 \pm 0.0596$ | $0.0749 \pm 0.00164$ | $1.66 \pm 0.0289$ | $0.283 \pm 0.0361$ | $0.155 \pm 0.0186$ | $36.3 \pm 4.76$ |
| ACM: | | | | | | |
| EQ | $0.737 \pm 0.0388$ | $6.053 \pm 0.785$ | $90.5 \pm 4.30$ | $40.3 \pm 4.28$ | $41.1 \pm 7.26$ | $-0.035 \pm 0.144$ |
| NEQ | $0.731 \pm 0.0616$ | $7.082 \pm 0.891$ | $189.0 \pm 8.65$ | $98.5 \pm 13.6$ | $61.9 \pm 6.07$ | $23.37 \pm 2.83$ |

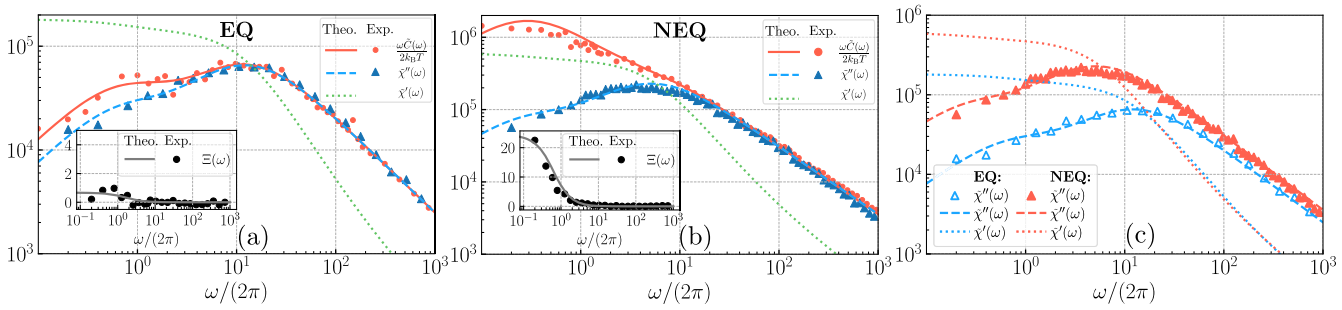


FIG. 1. RBC flickering. Comparison of experimental data (symbols) [20] and our model predictions for the tracer positional autocorrelation function $\omega\tilde{C}(\omega)/(2k_BT)$ in Eq. (9) (solid lines) and the imaginary part of the response function $\tilde{\chi}''(\omega)$ Eq. (8) (broken lines) for (a) the EQ scenario, i.e., ATP-depleted RBCs, and (b) the NEQ scenario, i.e., RBCs in the presence of ATP. In the insets, the spectral function $\Xi(\omega)$ from the experiments (symbols) is compared with our analytical prediction Eq. (10). (c) Comparison of the real and imaginary parts of the response function $\tilde{\chi}'(\omega)$ and $\tilde{\chi}''(\omega)$ for the NEQ and EQ scenarios, indicating a larger response (i.e., a softening) in the NEQ case in particular at low frequencies. The dotted lines in all subfigures indicate the model prediction for the real part of the response function $\tilde{\chi}'(\omega)$.

$\omega\tilde{C}(\omega)/(2k_BT)$ for both EQ and NEQ scenarios in the entire frequency range. The viscoelastic power-law exponents for NEQ and EQ turn out to be $\kappa = 0.936$ and $\kappa = 0.926$ (see Table I), respectively, rather close to viscous behavior ($\kappa = 1$). We also show the real (storage) part of the response function $\tilde{\chi}'(\omega)$ from our model as dotted lines in Figs. 1(a)–1(c), see Supplemental Material, Sec. V [46], for the explicit expression. In the EQ case $\tilde{\chi}''(\omega)$ and $\omega\tilde{C}(\omega)/(2k_BT)$ agree rather nicely and display a shoulder around $\omega/(2\pi) = 1\ \mathrm{s}^{-1}$, which in Supplemental Material, Sec. VII [46] is suggested to be caused by competing elastic and friction effects. In contrast, in the NEQ case the scaled autocorrelation $\omega\tilde{C}(\omega)/(2k_BT)$ is much larger than the response function $\tilde{\chi}''(\omega)$, indicating strong FDT violation. The spectral function $\Xi(\omega)$ in the insets illustrates that FDT violation occurs predominantly at low frequencies. The comparison in Fig. 1(c) demonstrates that both real and imaginary parts of the response function increase for NEQ at low frequencies, i.e., the effective stiffness of the network decreases at NEQ, this means that NEQ not only changes the active gel temperature but also the viscous and elastic model parameters. Indeed, the fitted tracer stiffness $K$ in Table I in the NEQ case is only one-third of the EQ scenario, which reflects NEQ-induced gel softening. Likewise, the elastic tracer-gel coupling $\hat{k}$ goes down in NEQ. In fact, the tracer friction coefficient $\gamma$ is comparable to the experimentally reported value for the bare tracer bead $\gamma = 0.085\ \mathrm{pN\,s/\mu m}$ [20] for NEQ and slightly increases for the EQ scenario, the gel friction coefficient $\hat{\gamma}_a$ is of the same order. Thus, all fit parameters of our model make physical sense. The nonequilibrium parameter in the NEQ case is $\alpha = 36$ and thus indicates strong departure from EQ. In the EQ case we obtain a finite value $\alpha \simeq 0.985$, which indicates weak NEQ due to incomplete ATP depletion in the experiment, as reflected by the weak deviation between the experimental $\tilde{\chi}''(\omega)$ and $\omega\tilde{C}(\omega)/(2k_BT)$ seen in Fig. 1(a).

Mizuno *et al.* [13] have studied the *in vitro* mechanics of active cross-linked actomyosin networks in the presence and absence of ATP, again referred to as NEQ and EQ cases, where the myosin-II motor proteins in the presence of ATP induce sliding motion between filaments connected by motors and thereby produce contractile active forces in the gel. As shown in Figs. 2(a) and 2(b), we again find excellent agreement between the experimental data and our

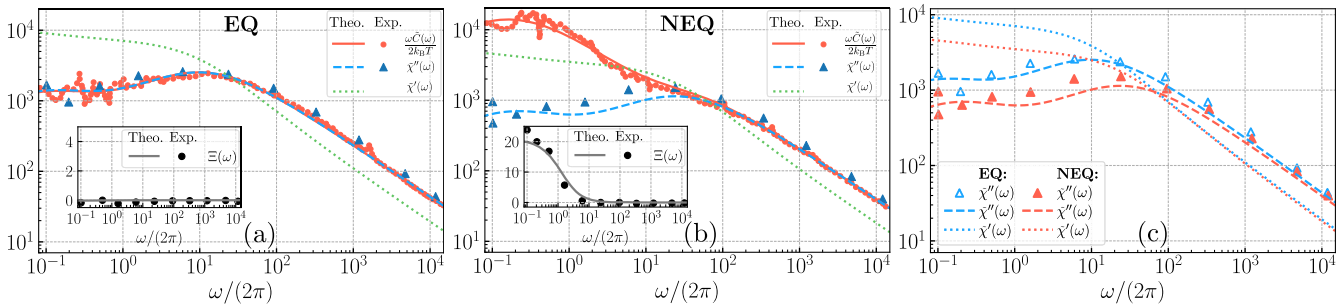


FIG. 2. Actomyosin networks. In analogy to Fig. 1, here we compare our model predictions for $\omega\tilde{C}(\omega)/(2k_BT)$ and $\tilde{\chi}''(\omega)$ (solid and broken curves) with experimental actomyosin-network data from Ref. [13] in the (a) absence and (b) presence of ATP. The insets show the spectral function $\Xi(\omega)$ defined in Eq. (7). (c) Actomyosin networks exhibit a decrease of the real and imaginary response $\tilde{\chi}'(\omega)$ and $\tilde{\chi}''(\omega)$ in NEQ.

fits for $\tilde{\chi}''(\omega)$ and $\omega\tilde{C}(\omega)/(2k_BT)$ for both the EQ and the NEQ scenarios in the entire frequency range. In the EQ case $\tilde{\chi}''(\omega)$ and $\omega\tilde{C}(\omega)/(2k_BT)$ are practically identical and show (similar to RBC) two weak maxima that are well produced by our model, see Supplemental Material, Sec. VII [46], for an asymptotic analysis. In the NEQ case the scaled autocorrelation $\omega\tilde{C}(\omega)/(2k_BT)$ is much larger than the response function $\tilde{\chi}''(\omega)$, indicating strong FDT violation characterized by $\alpha = 23.4$, rather similar to the RBC case. In the absence of ATP the fit value $\alpha = -0.035$ indicates almost perfect EQ behavior. For both EQ and NEQ scenarios the fitted power-law exponent in Table I is in excellent agreement with $\kappa = 3/4$ predicted by theory [1,10,56] and experiments [13]. In Supplemental Material, Sec. VIII [46], we propose a simple microscopic model consisting of a bead attached to elastic filaments which not only produces the power-law scaling $\chi''(\omega) \sim \omega^{-3/4}$ in the high-frequency regime but also relates the effective parameters $\gamma$ and $K$ to parameters of the microscopic model.

The comparison in Fig. 2(c) demonstrates that both real and imaginary parts of the response function are at low frequencies for NEQ smaller than for EQ, i.e., the effective stiffness of the network increases in the NEQ case, in contrast to the RBC experiments. This different behavior is primarily caused by the elastic model parameters: Table I shows that $K$, the tracer stiffness, and $\hat{k}$, the tracer-gel elastic coupling strength, increase for actomyosin networks when going from EQ to NEQ, whereas the opposite trend is observed for the RBC flickering data.

In summary, our simple model for viscoelastic active biomatter incorporates the elastic coupling between a tracer bead and an active viscoelastic medium and yields closed-form analytical predictions for the tracer autocorrelation and response function which are in excellent agreement with experimental data for RBCs and actomyosin networks. Our model quantifies the departure from EQ by the NEQ parameter $\alpha$, which corresponds to the gel-tracer effective temperature ratio. We find $\alpha \approx 23$, 36 in the presence of ATP and $\alpha \approx 0$, 1 in the absence of ATP for the two experimental systems we considered, respectively, clearly signaling the strong NEQ character induced by ATP. Note that the effective temperature of the active gel does not correspond to its actual physical temperature, but rather characterizes the strength of its stochastic force and the power it dissipates. The comparison of our model with a more detailed model for the active gel that includes an active colored noise term [21] in Supplemental Material, Sec. III [46], is revealing: the salient deviation between the tracer correlation function and the tracer response function at low frequencies in the experimental data in Figs. 1 and 2 is rather independent of details of the nonequilibrium gel properties. Thus, the spectral violation of the fluctuation dissipation theorem in the experimental data is dominated by the viscoelastic coupling between the tracer particle and the active gel. Our power-law model introduced in the main text, the exponentially correlated active noise model in the Supplemental Material, Sec. III, [46], and the method for direct extraction of the memory kernel in Supplemental Material, Sec. II, [46], can be straightforwardly applied to other experimental setups and diverse non-equilibrium biomaterials such as tissue and multicellular systems.

A. A. and R. R. N. acknowledge Hélène Berthoumieux for useful discussions, the European Research Council (ERC) Advanced Grant No. MaMemo Grant No. 835117, the Deutsche Forschungsgemeinschaft (DFG, German Research Foundation) Project ID 431232613—SFB 1449. A. A. acknowledges the hospitality by the Institute for Research in Fundamental Sciences (IPM), Tehran. A. N. acknowledges support from the ICTP (Trieste, Italy) through the Associates Programme and from Simon Foundation through Grant No. 284558FY19.

*a.naji@ipm.ir

[1] B. Schnurr, F. Gittes, F. C. MacKintosh, and C. F. Schmidt, Macromolecules **30**, 7781 (1997).
[2] J. Joanny and J. Prost, HFSP J. **3**, 94 (2009).
[3] Y. Osada and J.-P. Gong, Adv. Mater. **10**, 827 (1998).
[4] A. D. Bershadsky and J. M. Vasiliev, *Cytoskeleton* (Springer Science & Business Media, New York, 2012).
[5] E. L. Elson, Annu. Rev. Biophys. Biophys. Chem. **17**, 397 (1988).
[6] F. Jülicher, K. Kruse, J. Prost, and J.-F. Joanny, Phys. Rep. **449**, 3 (2007).
[7] D. A. Fletcher and R. D. Mullins, Nature (London) **463**, 485 (2010).
[8] O. Lieleg, M. M. Claessens, and A. R. Bausch, Soft Matter **6**, 218 (2010).
[9] O. Pelletier, E. Pokidysheva, L. S. Hirst, N. Bouxsein, Y. Li, and C. R. Safinya, Phys. Rev. Lett. **91**, 148102 (2003).
[10] T. Hiraiwa and R. R. Netz, Europhys. Lett. **123**, 58002 (2018).
[11] I. Rayment, H. Holden, M. Whittaker, C. Yohn, M. Lorenz, K. Holmes, and R. Milligan, Science **261**, 58 (1993).
[12] A. C. Martin, M. Kaschube, and E. F. Wieschaus, Nature (London) **457**, 495 (2009).
[13] D. Mizuno, C. Tardin, C. F. Schmidt, and F. C. MacKintosh, Science **315**, 370 (2007).
[14] J. Mills, L. Qie, M. Dao, C. Lim, and S. Suresh, MCB Mol. Cell. Biomech. **1**, 169 (2004).
[15] M. Puig-de Morales-Marinkovic, K. T. Turner, J. P. Butler, J. J. Fredberg, and S. Suresh, Am. J. Physiol. Cell Physiol. **293**, C597 (2007).
[16] S. Tuvia, A. Almagor, A. Bitler, S. Levin, R. Korenstein, and S. Yedgar, Proc. Natl. Acad. Sci. U.S.A. **94**, 5045 (1997).
[17] M. D. E. A. Faris, D. Lacoste, J. Pécréaux, J.-F. Joanny, J. Prost, and P. Bassereau, Phys. Rev. Lett. **102**, 038102 (2009).
[18] T. Betz and C. Sykes, Soft Matter **8**, 5317 (2012).
[19] P. Girard, J. Prost, and P. Bassereau, Phys. Rev. Lett. **94**, 088102 (2005).

[20] H. Turlier, D. A. Fedosov, B. Audoly, T. Auth, N. S. Gov, C. Sykes, J.-F. Joanny, G. Gompper, and T. Betz, Nat. Phys. **12**, 513 (2016).
[21] A. Bernheim-Groswasser, N. S. Gov, S. A. Safran, and S. Tzlil, Adv. Mater. **30**, 1707028 (2018).
[22] J. O. Rädler, T. J. Feder, H. H. Strey, and E. Sackmann, Phys. Rev. E **51**, 4526 (1995).
[23] J.-B. Manneville, P. Bassereau, D. Lévy, and J. Prost, Phys. Rev. Lett. **82**, 4356 (1999).
[24] D. Mizuno, D. Head, F. MacKintosh, and C. Schmidt, Macromolecules **41**, 7194 (2008).
[25] T. Betz, M. Lenz, J.-F. Joanny, and C. Sykes, Proc. Natl. Acad. Sci. U.S.A. **106**, 15320 (2009).
[26] Y. Park, C. A. Best, T. Auth, N. S. Gov, S. A. Safran, G. Popescu, S. Suresh, and M. S. Feld, Proc. Natl. Acad. Sci. U.S.A. **107**, 1289 (2010).
[27] R. Mauri and D. Leporini, Europhys. Lett. **76**, 1022 (2006).
[28] L. Berthier and J.-L. Barrat, J. Chem. Phys. **116**, 6228 (2002).
[29] G. Szamel, Phys. Rev. E **90**, 012111 (2014).
[30] T. S. Grigera and N. E. Israeloff, Phys. Rev. Lett. **83**, 5038 (1999).
[31] E. Fodor, C. Nardini, M. E. Cates, J. Tailleur, P. Visco, and F. van Wijland, Phys. Rev. Lett. **117**, 038103 (2016).
[32] E. Ben-Isaac, Y. Park, G. Popescu, F. L. H. Brown, N. S. Gov, and Y. Shokef, Phys. Rev. Lett. **106**, 238103 (2011).
[33] N. Gov, A. G. Zilman, and S. Safran, Phys. Rev. Lett. **90**, 228101 (2003).
[34] R. Rodríguez-García, I. López-Montero, M. Mell, G. Egea, N. S. Gov, and F. Monroy, Biophys. J. **108**, 2794 (2015).
[35] N. S. Gov and S. A. Safran, Biophys. J. **88**, 1859 (2005).
[36] L. C.-L. Lin, N. Gov, and F. L. H. Brown, J. Chem. Phys. **124**, 074903 (2006).
[37] R. R. Netz, J. Chem. Phys. **148**, 185101 (2018).
[38] U. S. Schwarz and S. A. Safran, Rev. Mod. Phys. **85**, 1327 (2013).
[39] I. Goychuk, Adv. Chem. Phys. **150**, 187 (2012).
[40] F. Mainardi, in *Fractals and Fractional Calculus in Continuum Mechanics* (Springer, New York, 1997), p. 291.
[41] B. Fabry, G. N. Maksym, J. P. Butler, M. Glogauer, D. Navajas, and J. J. Fredberg, Phys. Rev. Lett. **87**, 148102 (2001).
[42] P. Bursac, B. Fabry, X. Trepat, G. Lenormand, J. P. Butler, N. Wang, J. J. Fredberg, and S. S. An, Biochem. Biophys. Res. Commun. **355**, 324 (2007).
[43] M. Costa, I. Ghiran, C.-K. Peng, A. Nicholson-Weller, and A. L. Goldberger, Phys. Rev. E **78**, 020901(R) (2008).
[44] J. Kappler, F. Noé, and R. R. Netz, Phys. Rev. Lett. **122**, 067801 (2019).
[45] A. Taloni, A. Chechkin, and J. Klafter, Phys. Rev. Lett. **104**, 160602 (2010).
[46] See Supplemental Material at http://link.aps.org/supplemental/10.1103/PhysRevLett.131.228202 for derivations of all equations in the main text and details of the method used to fit the model predictions to the experimental data. We also provide results for alternative viscoelastic models such as the Maxwell and the Kelvin-Voigt model. Also, we provide results for the power-law memory kernel with exponentially correlated active noise and a minimalistic model to describe the positional response of a tracer in a polymeric network. We also introduce a method to extract the memory from experimental data on response function. The Supplemental Material includes Refs. [47–54].
[47] C. H. Wiggins, D. Riveline, A. Ott, and R. E. Goldstein, Biophys. J. **74**, 1043 (1998).
[48] C. Duprat and H. A. Stone, *Fluid-Structure Interactions in Low-Reynolds-Number Flows* (Royal Society of Chemistry, Cambridge, 2015).
[49] T. R. Powers, Rev. Mod. Phys. **82**, 1607 (2010).
[50] G. K. Batchelor, J. Fluid Mech. **44**, 419 (1970).
[51] J. K. Dhont, *An Introduction to Dynamics of Colloids* (Elsevier, New York, 1996).
[52] J. Howard, *Mechanics of Motor Proteins and the Cytoskeleton* (Sinauer Associates, Sunderland, 2001).
[53] W. H. Press, S. A. Teukolsky, W. T. Vetterling, and B. P. Flannery, *Numerical Recipes 3rd Edition: The Art of Scientific Computing* (Cambridge University Press, Cambridge, England, 2007).
[54] A. Rohatgi, Webplotdigitizer: Version 4.4 (2020).
[55] R. Kubo, M. Toda, and N. Hashitsume, *Statistical Physics II: Nonequilibrium Statistical Mechanics* (Springer-Verlag, Berlin, 1991), Vol. 31.
[56] D. C. Morse, Phys. Rev. E **58**, R1237 (1998).